International Journal of Nanomedicine

Dovepress
open access to scientific and medical research

Open Access Full Text Article

ORIGINAL RESEARCH

Activation of Dynamin-Related Protein 1 and Induction of Mitochondrial Apoptosis by Exosome-Rifampicin Nanoparticles Exerts Anti-Osteosarcoma Effect

Wenkai Chen[1,2,*], Wenping Lin[3,*], Naichun Yu[1,2,*], Linlin Zhang[1,2,*], Zuoxing Wu[2], Yongjie Chen[1,2], Zongguang Li[1,2], Fengqing Gong[1,2], Na Li[2], Xiaohui Chen[4], Xu He[3], Yue Wu[5], Xiangchen Zeng[1,2], Yuting Yueh[1,2], Ren Xu[2,4,6,*], Guangrong Ji[1,2,*]

[1]Department of Orthopedic Surgery, Xiang'an Hospital of Xiamen University, School of Medicine, Xiamen University, Xiamen, People's Republic of China; [2]Fujian Provincial Key Laboratory of Organ and Tissue Regeneration, Xiamen Key Laboratory of Regeneration Medicine, Organ Transplantation Institute of Xiamen University, School of Medicine, Xiamen University, Xiamen, People's Republic of China; [3]Department of Spine Surgery, Shenzhen Pingle Orthopedic Hospital, Affiliated Hospital of Guangzhou University of Traditional Chinese Medicine, Shenzhen, People's Republic of China; [4]Department of Orthopedic Surgery, The First Affiliated Hospital of Xiamen University, Xiamen, People's Republic of China; [5]Department of Pathology, Zhongshan Hospital, Xiamen University, Xiamen, People's Republic of China; [6]Collaborative Innovation Centre of Regenerative Medicine and Medical BioResource Development and Application Co-Constructed by the Province and Ministry, Guangxi Medical University, Nanning, People's Republic of China

*These authors contributed equally to this work

Correspondence: Guangrong Ji; Ren Xu, Department of Orthopedic Surgery, Xiang'an Hospital of Xiamen University, No. 2000, Xiang'an East Road, Xiang'an District, Xiamen, 361000, People's Republic of China, Tel +86-15710667257, Fax +86592-2889000, Email jiguangrong@xmu.edu.cn; xuren526@xmu.edu.cn

Purpose: To investigate induction of cell death in Osteosarcoma (OS) using the anti-tuberculosis drug, rifampicin, loaded into exosomes.

Patients and Methods: BMSC-exosomes were isolated by ultracentrifugation and loaded ultrasonically with rifampicin. Nanoparticle exosome-rifampicin (EXO-RIF) was added to the OS cell-lines, 143B and MG63, in vitro, to observe the growth inhibitory effect. In vivo experiments were conducted by injecting fluorescently labeled EXO-RIF through the tail vein of 143B cell xenograft nude mice and tracking distribution. Therapeutic and toxic side-effects were analyzed systemically.

Results: Sonication resulted in encapsulation of rifampicin into exosomes. Exosome treatment accelerated the entry of rifampicin into OS cells and enhanced the actions of rifampicin in inhibiting OS proliferation, migration and invasion. Cell cycle arrest at the G2/M phase was observed. Dynamin-related protein 1 (Drp1) was activated by EXO-RIF and caused mitochondrial lysis and apoptosis. Exosome treatment targeted rifampicin to the site of OS, causing OS apoptosis and improving mouse survival in vivo.

Conclusion: The potent Drp1 agonist, rifampicin, induced OS apoptosis and exosome loading, improving OS targeting and mouse survival rates. EXO-RIF is a promising strategy for the treatment of diverse malignancies.

Keywords: bone tumor, drug delivery, exosomes, mesenchymal stem cells, survival

Introduction

Osteosarcoma (OS) is the most common primary bone malignancy in children and adolescents and has the highest incidence of any primary soft tissue malignancy.[1,2] Significant progress has been made in OS diagnosis and treatment due to advances in surgery and chemotherapy.[3–5] The combination of margin-negative surgical resection in conjunction with triple-drug chemotherapy is an effective treatment and it is now recognized that up to 90% of OS cases have at least micrometastatic disease at the time of diagnosis. Nonetheless, 5-year progression-free survival rates of recurrent and

Received: 24 June 2022
Accepted: 12 November 2022
Published: 18 November 2022

Graphical Abstract

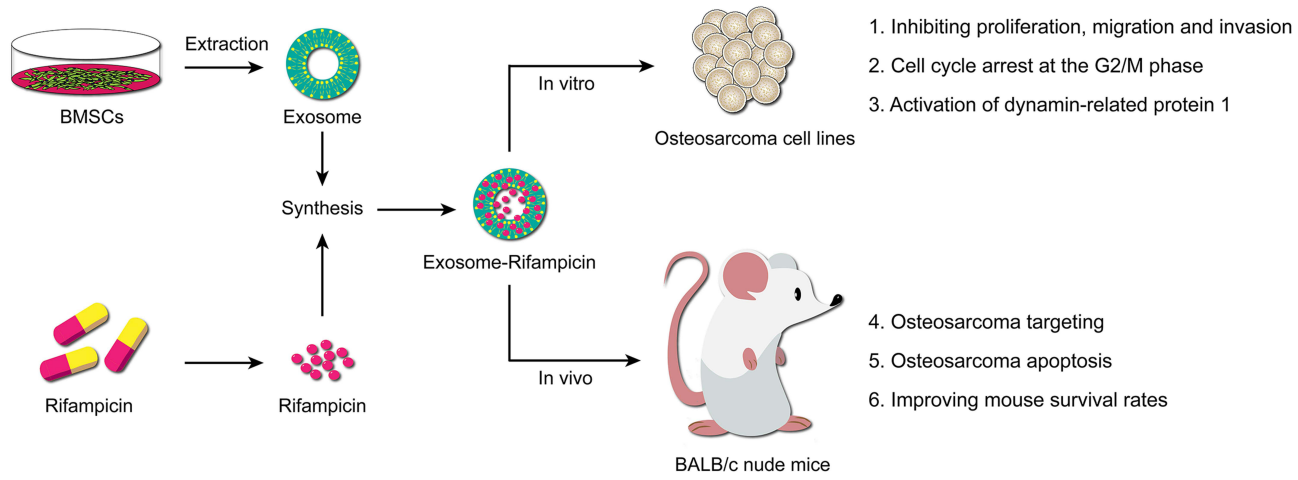

metastatic OS are still below 30%.[6,7] Therefore, there is an urgent need to explore new therapeutic strategies with special emphasis on anti-OS drugs.

Rifampicin is a traditional anti-tuberculosis drug, in use since 1966,[10] which exerts its antibacterial effect by binding to the β-subunit of DNA-dependent bacterial RNA polymerase, inhibiting transcription.[8,9] Large-scale drug screening has demonstrated the anti-OS activity of rifampicin which causes mitochondrial lysis, inducing apoptosis and cell cycle arrest.

Exosomes (EXO) are extracellular vesicles secreted by mesenchymal stem cells (MSCs) which retain the tumor-regulating properties of the parent cells.[11] EXO transport proteins, lipids and RNA through physiological barriers, including the blood–brain barrier, into target cells to achieve intercellular communication and regulation.[12–14] The small size, low immunogenicity, good biocompatibility and excellent tumor targeting properties of MSC-EXO make them an optimal choice for in vivo anti-tumor drug delivery. Consequently, there has been much interest in developing this therapeutic approach.[15–17]

Rifampicin was loaded into EXO derived from bone marrow stem/stromal cells (BMSCs) and administered intravenously to OS xenograft models during the current study. Exosome-rifampicin (EXO-RIF) was demonstrated to activate dynamin-related protein 1 (Drp1) and induce mitochondrial apoptosis, resulting in potent anti-tumor therapeutic effects. Toxicity was found to be low, making EXO-RIF a promising new strategy for treatment of malignant tumors.

Materials and Methods

Cell Culture

The human OS cell lines, 143B and MG63 (Procell, China), were cultured in Dulbecco's Modified Eagle Medium (DMEM) with high glucose (Hyclone, USA) supplemented with 10% fetal bovine serum (HyClone, USA) and 1% penicillin/streptomycin (HyClone, USA). Human BMSCs (Hm-BMSCs, Procell, China) were cultured in alpha-MEM (Hyclone, USA) supplemented with 10% fetal bovine serum (HyClone, USA) and 1% penicillin/streptomycin (HyClone, USA). All cells were cultured at 37°C in 5% CO_2.

Preparation of Exosomes

EXO were purified as described previously with modifications.[18] Conditioned cell culture medium containing EXO was centrifuged at 3000 g for 15 minutes to eliminate cells. The resulting supernatant was centrifuged for 60 minutes at

100,000 g, washed with cold PBS and centrifuged again at 100,000 g for 60 minutes. All centrifugations were performed at 4°C. EXO were resuspended in PBS and stored at −80°C.

EXO concentration was determined by protein content measured by Pierce BCA Protein Assay Kit (Thermo, USA). EXO were diluted to 1 mg/mL and size distribution analysis conducted using Mastersizer (Malvern, UK). Morphology was observed by transmission electron microscopy (Hitachi HT-7800, Japan) and expression of exosome markers, CD63, TSG101, CD9 and CD81, determined by Western blotting.

Drug Loading into Exosomes

Drug loading was performed as described previously.[19] Briefly, a mixture of EXO and rifampicin was sonicated with the following settings: 20% amplitude, 6 cycles of 30s on/off for three minutes with a two-minute cooling period between each cycle. The resulting EXO-RIF solution was incubated at 37°C for 60 min to allow recovery of the exosomal membrane and excess free drug removed from EXO-RIF by ultracentrifugation. The concentration of free rifampicin in the supernatant was measured by UV-Spectroscopy (Omega POLARstar, Germany) at the RF λmax (473 nm).

Drug Release Assay

Dialysis tubes were immersed in PBS at pH 7.4 or pH 4.5 and the in vitro drug release profile determined by transferring 3 mL of EXO-RIF solution into the tubes. RIF release into the bathing medium at 37°C was measured at 1, 2, 4, 6, 12, 18, 24, 36 and 48 h at the RF λmax (473 nm) by UV-Spectroscopy (Omega POLARstar, Germany).[20]

Flow Cytometry

Cells were grown in six-well plates for 24 h with different treatments, harvested and stained for 15 min with FITC-conjugated annexin V and propidium iodide (BD, USA) or for 30 min with 10 μg/mL JC-1 (Thermo Fisher Scientific, USA). Cells were fixed in cold 70% ethanol overnight at −20°C and stained with propidium iodide for cell cycle analysis. Flow cytometry was performed (Beckman Cytoflex LX, USA) and data analyzed by CytExpert software.

Cytotoxicity Assay

Aliquots of 1×10^4 cells/well were plated into 96-well plates, cultivated with treatments as indicated and absorbance of reduced WST-8 at 450 nm measured at each time point to calculate the number of cells in three replicate wells.

Colony Formation

Colony formation was measured as described previously.[21] Six-well plates were seeded with 200 cells/well, cultured for 7 days and fixed for 20 minutes with ice-cold methanol before staining with crystal violet. Colonies with >50 cells were counted under an optical microscope (Carl Zeiss, Germany).

Wound Healing Assay

Briefly, 5×10^5 cells were cultured in six-well plates for 24 hours and monolayers scratched with a 200 μL sterile pipette. Photographs were taken 24 hours later. The experiment was repeated three times.

Transwell Assay

The upper chamber was precoated with Matrigel solution for 2 h (Corning, Australia) and 1×10^5 cells/well cultured in 100 μL FBS-free medium with 600 μL complete medium added to the lower chamber. Non-migrating cells remaining on the upper side of the chamber were removed after 24 h and invasive cells in the lower chamber were fixed with methanol for 20 min and stained with 0.1% crystal violet (Solarbio, China) for 30 min before counting under an inverted microscope.

RNA Sequencing

Total RNA was isolated from three different OS cells in TRIzol, RNA-sequencing (RNA-Seq) performed and data analyzed at the UAB Genomics Core Facility. RNA-Seq was carried out on the Illumina NextSeq500, according to the manufacturer's protocol (Illumina Inc., San Diego, CA).

Intracellular ROS Measurements

Intracellular ROS were measured using DCFDA/H2DCFDA-Cellular ROS Assay Kit (Abcam, USA) and MitoSOX (Yeasen, China). In brief, cells were incubated with 20 μM DCFDA or 5 μM MitoSOX for 30 min at 37°C, washed with PBS and fluorescence detected by Olympus BX50 fluorescence microscope.

Western Blot Analysis

Equal amounts of protein per well were separated by 8–12% sodium dodecyl sulfate-polyacrylamide gel electrophoresis and transferred to polyvinylidene fluoride membranes (Millipore, USA). Membranes were incubated with primary antibodies raised against the following proteins: β-Actin (1:3000, Cat#ab20272, Abcam), CD63 (1:1000, Cat#ab68418, Abcam), TSG101 (1:1000, Cat#ab125011, Abcam), CD9 (1:1000, Cat#ab236630, Abcam), CD81 (1:1000, Cat#ab79559, Abcam), Calnexin (1:1000, Cat#ab22595, Abcam), PARP1 (1:1000, Cat#ab32064, Abcam), Caspase3 (1:1000, Cat#ab32351, Abcam), Cleaved-Caspase-9 (1:1000, Cat#ab2324, Abcam), Bcl-2 (1:1000, Cat#ab182858, Abcam), Bcl-xl (1:1000, Cat#ab32370, Abcam), Bax (1:1000, Cat#ab32503, Abcam), Bad (1:1000, Cat#ab32445, Abcam), Cytochrome C (1:1000, Cat#ab133504, Abcam), AIF (1:1000, Cat#ab32516, Abcam), COX-IV (1:1000, Cat#ab33985, Abcam), Drp1 (1:1000, Cat#ab184247, Abcam), Phospho-Drp1 (1:1000, Cat#3455, CST), Fis1 (1:1000, Cat#ab96764, Abcam), Opa1 (1:1000, Cat#ab157457, Abcam), Ndufs1 (1:1000, Cat#12444-1-AP, Proteintech), Sdha (1:1000, Cat#14865-1-AP, Proteintech), Mfn1 (1:1000, Cat#14739, CST), Uqcrc1 (1:1000, Cat#21705-1-AP, Proteintech), ATP5A (Cat#14676-1-AP, Proteintech), Mfn2 (1:1000, Cat#11925, CST) and Ki67 (1:1000, Cat# ab16667, Abcam).

Cellular ATP Levels

ATP was measured by kit, according to the manufacturer's instructions (Beyotime, China). Cells were grown in 6-well plates, lysate added and medium centrifuged at 12,000 g for 5 min. ATP concentration was measured in the supernatant by reference to a standard curve.

Animal Experiments

Male BALB/c nude mice (4-week-old) were provided by Xiamen University Laboratory Animal Center (Xiamen, China) and housed with an air filter cover under a 12 h light/12 h dark cycle and temperature-controlled (24 ± 1°C) environment. 143B cells (2×10^6 /10 μL) were injected into the right tibia under anesthesia to construct the nude mouse OS model, allowed to grow for 7 days and saline with exosome (1×10^8/mL) and rifampicin (10 mg/kg) injected through the tail vein. Ethical approval was granted by Xiamen University Laboratory Animal Management and Ethics Committee in accordance with the guidelines on animal welfare of the Chinese Society of Laboratory Animals.

Micro-Computed Tomography (CT) Analysis

Tibia were scanned with micro-CT (SkyScan, United States) and three-dimensional (3D) reconstructions generated by NRecon program. Testing parameters were 60 kV (source voltage), 160 μA (source current), rotation step of 0.4°, AI 0.25 mm filter and a pixel size of 10 μm.

TUNEL Staining

Apoptosis in tumor tissue was assessed by TUNEL staining. Frozen sections were fixed with paraformaldehyde for 30 min and incubated with PBS containing 0.5% Triton X-100 at room temperature for 5 min. TUNEL detection solution was added, sections incubated at 37°C for 60 min in the dark, washed with PBS three times, anti-fluorescence quenching mounting solution added dropwise and fluorescence observed under a microscope.

Cytotoxicity Evaluation

Alanine transaminase (ALT), aspartate transaminase (AST), blood urea nitrogen (BUN), creatinine (Cr), creatine kinase (CK) and creatine kinase-MB (CK-MB) were measured in mouse serum. Heart, liver, spleen, lung and kidney were removed after sacrifice for H&E staining.

Statistical Analysis

Data are expressed as mean ± SEM. Student's *t*-test was used for two-group comparison and one-way ANOVA was used for comparison among more than two groups. Differences were considered statistically significant when the p value was < 0.05.

Results

Generation and Characterization of Exosome-Rifampicin

EXO were isolated from BMSCs by ultracentrifugation (Figure 1B) and RIF loaded into exosomes ultrasonically (Figure 1A). Freshly extracted EXO had diameters of approximately 50–150 nm and after sonication, diameters were about 65–225 nm (Figure 1C and D), as determined by transmission electron microscopy and rice particle tracking. EXO and EXO-RIF expressed exosome-specific antigens, CD63/TSG101/CD9/CD81, but did not express the endoplasmic reticulum-specific antigen, calnexin, and had low expression of β-actin, as shown by Western blotting (Figure 1E).

The drug release rate from EXO-RIF was significantly higher at pH 4.5 than at pH 7.4, suggesting higher release in an acidic environment (Figure 1F).

EXO and EXO-RIF particle sizes did not change significantly when stored at −20 C for 28 days (Figure 1G).

Cellular Uptake of Exosomes in vitro

Both RIF and CY3 fluorescence labelled RIF (Figure S1) had similar anti-OS efficacy (Figure S2). RIF-CY3 was loaded into exosomes labeled with PKH-67 (Figure 2A).

Flow cytometry of fluorescent 143B cells showed that exosome encapsulation significantly promoted the entry of RIF-CY3 into cells (Figure 2B and C) and RIF loading did not affect the rate of exosome entry into cells (Figure 2D and E). Fluorescence microscopy confirmed the above findings (Figure 2F and G).

Anti-OS Effect of EXO-RIF in vitro

EXO-RIF without CY3 labeling (Figure 3A) inhibited OS proliferation and had a cytotoxic effect (Figure 3B). RIF, itself, inhibited OS cell migration and this effect was more potent in the form of EXO-RIF (Figures 3C and S3). Both RIF and EXO-RIF inhibited tumor cell colony formation (Figures 3D and S4). RIF inhibited OS cell invasion and this effect was more potent in the form of EXO-RIF (Figures 3E and S5). Flow cytometry showed that RIF caused OS cell cycle stagnation in the G2/M phase and this effect was more potent when EXO-RIF was used (Figures 3F and S6).

EXO-RIF Induced Mitochondrial Apoptosis of OS Cells

RNA-Seq suggested the involvement of mitophagy (Figure 4A–D) and mitochondria could be seen to shorten and become vacuolated after EXO-RIF treatment by transmission electron microscopy (Figure 5B). EXO-RIF may have caused mitochondrial dysfunction (Figure 5C) and apoptosis (Figure 5A) from flow cytometry analysis. EXO-RIF caused the accumulation of ROS, perhaps due to increased mitochondrial cleavage (Figure 5D). Cytochrome-C and apoptosis-inducing factor (AIF) from mitochondria were released into the cytoplasm in large quantities, leading to apoptosis (Figure 5E and F).

EXO-RIF Activated Phosphorylation of Drp1 Causing Excessive Mitochondrial Lysis

The mitochondrial morphology protein, Fis1, was increased and Opa1/Mfn1/Mfn2 were decreased after EXO-RIF treatment, as shown by immunoblots. More importantly, EXO-RIF induced Drp1 phosphorylation which moved from the cytoplasm to the mitochondria (Figure 6A and B). EXO-RIF was also found to cause mitochondrial inactivation (Figure 6C), deficient ATP production (Figure 6D) and decreased respiratory chain complex expression (Figure 6E). The inhibitor of Drp1 phosphorylation, Mdivi-1, reversed EXO-RIF-induced apoptosis and reduced mitochondrial ROS production (Figure 6F and G).

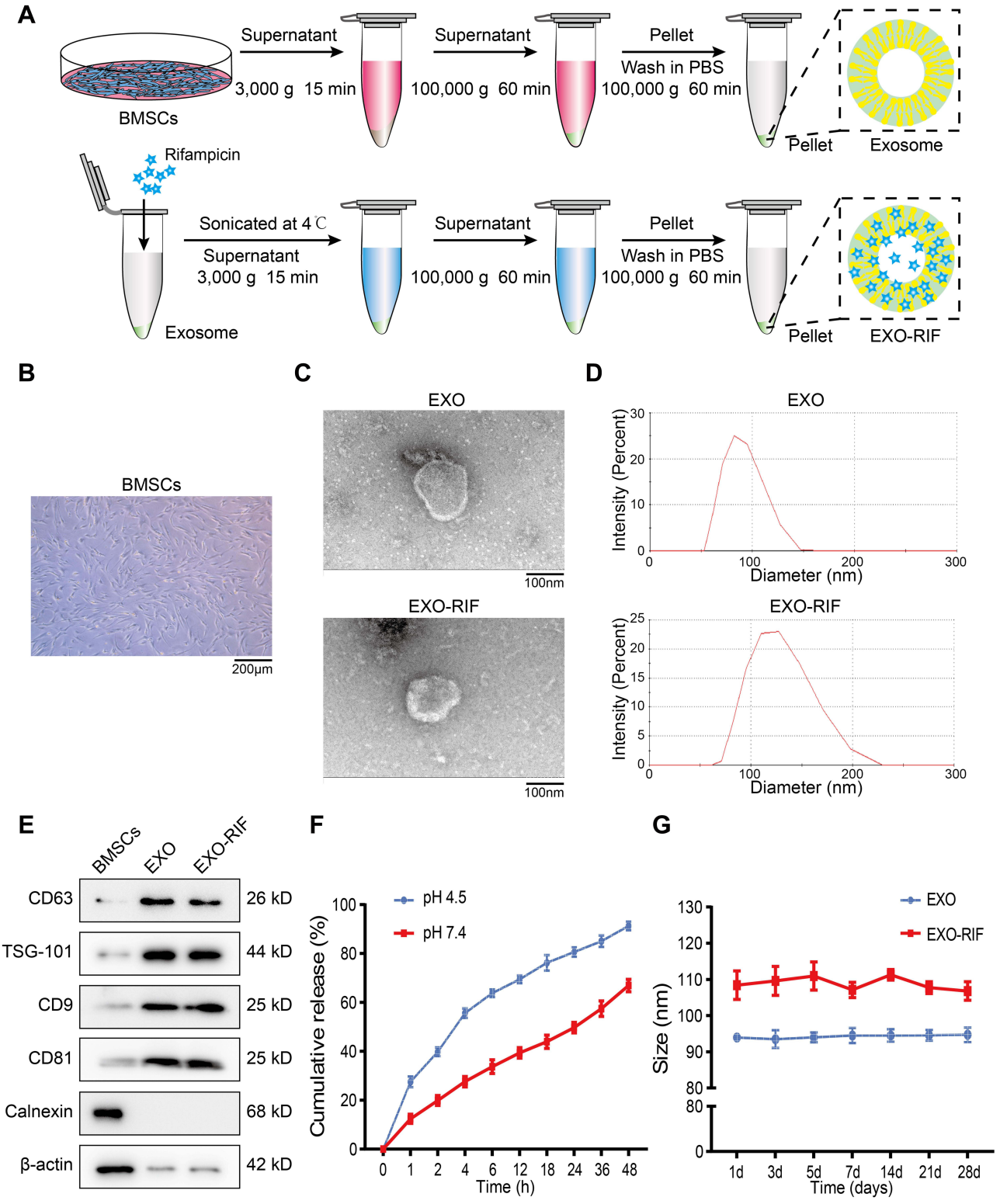

Figure 1 Preparation and characterization of Exosome-Rifampicin. (**A**) Schematic illustration of exosome preparation. (**B**) Representative images of BMSCs. (**C**) Representative images of transmission electron micrographs of Exosome and Exosome-Rifampicin. (**D**) Size distribution of Exosome and Exosome-Rifampicin. n = 3 samples per group. (**E**) Western blot analysis of exosome markers, CD63, TSG101, CD9, CD81, and Endoplamic reticulum marker, Calnexin, on BMSCs, Exosomes and Exosome-Rifampicin. (**F**) Drug release profile of Exosome-Rifampicin[22] in PBS with pH4.5 and pH7.4. (**G**) Particle size by nanoparticle tracking analysis for BMSC-derived exosomes and Exosome-Rifampicin during storage at −20 C.

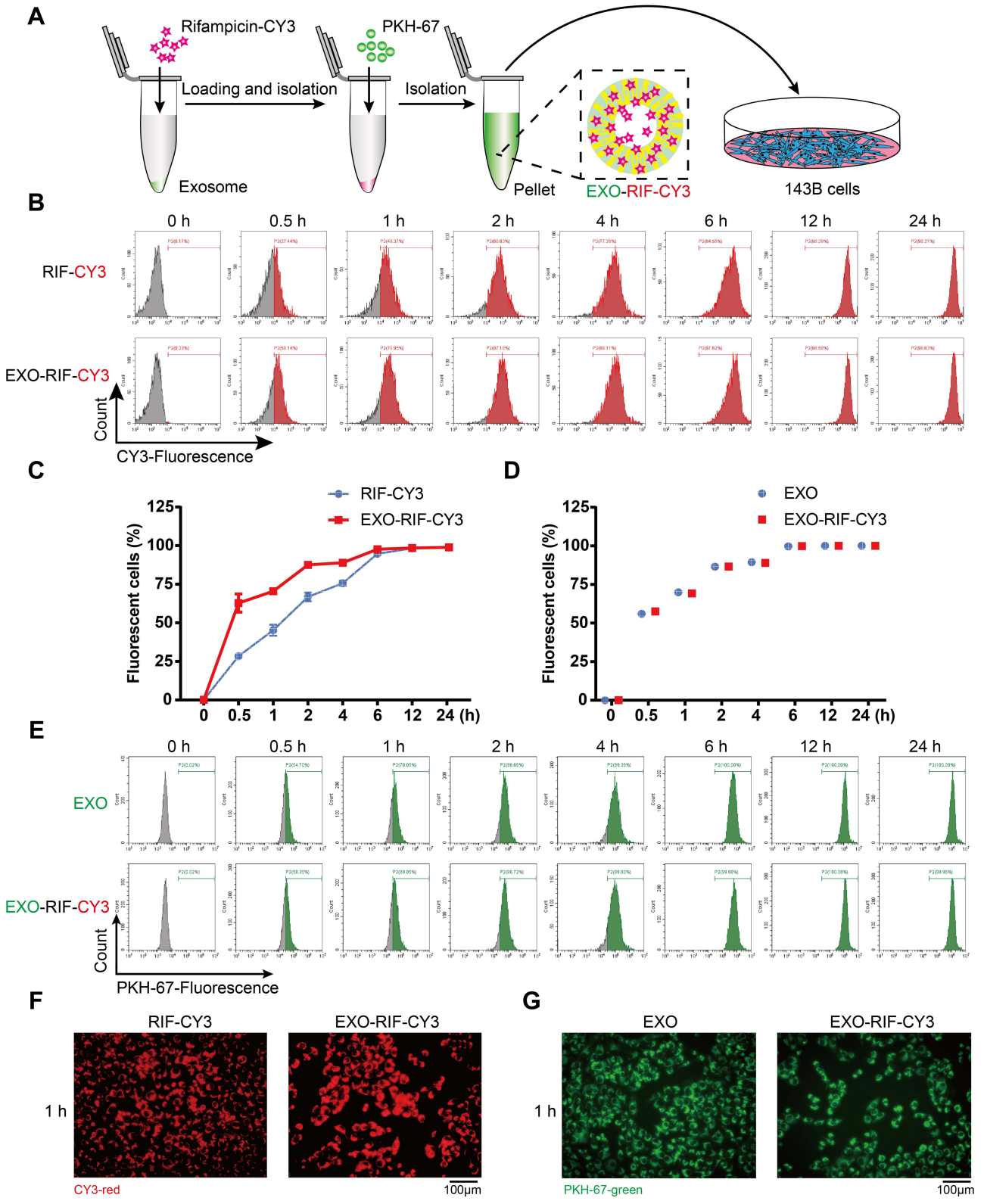

Figure 2 Exosome loading accelerated rifampicin entry into osteosarcoma cells. (**A**) Schematic illustration of the experiment. (**B** and **C**) CY3-Fluorescence of cells detected by flow cytometry. n = 3 samples per group. (**D** and **E**) PKH-67-Fluorescence of cells detected by flow cytometry. n = 3 samples per group. (**F** and **G**) Fluorescence microscopy to detect CY3-fluorescence and PKH-67-fluorescence in cells.

https://doi.org/10.2147/IJN.S379917 DovePress

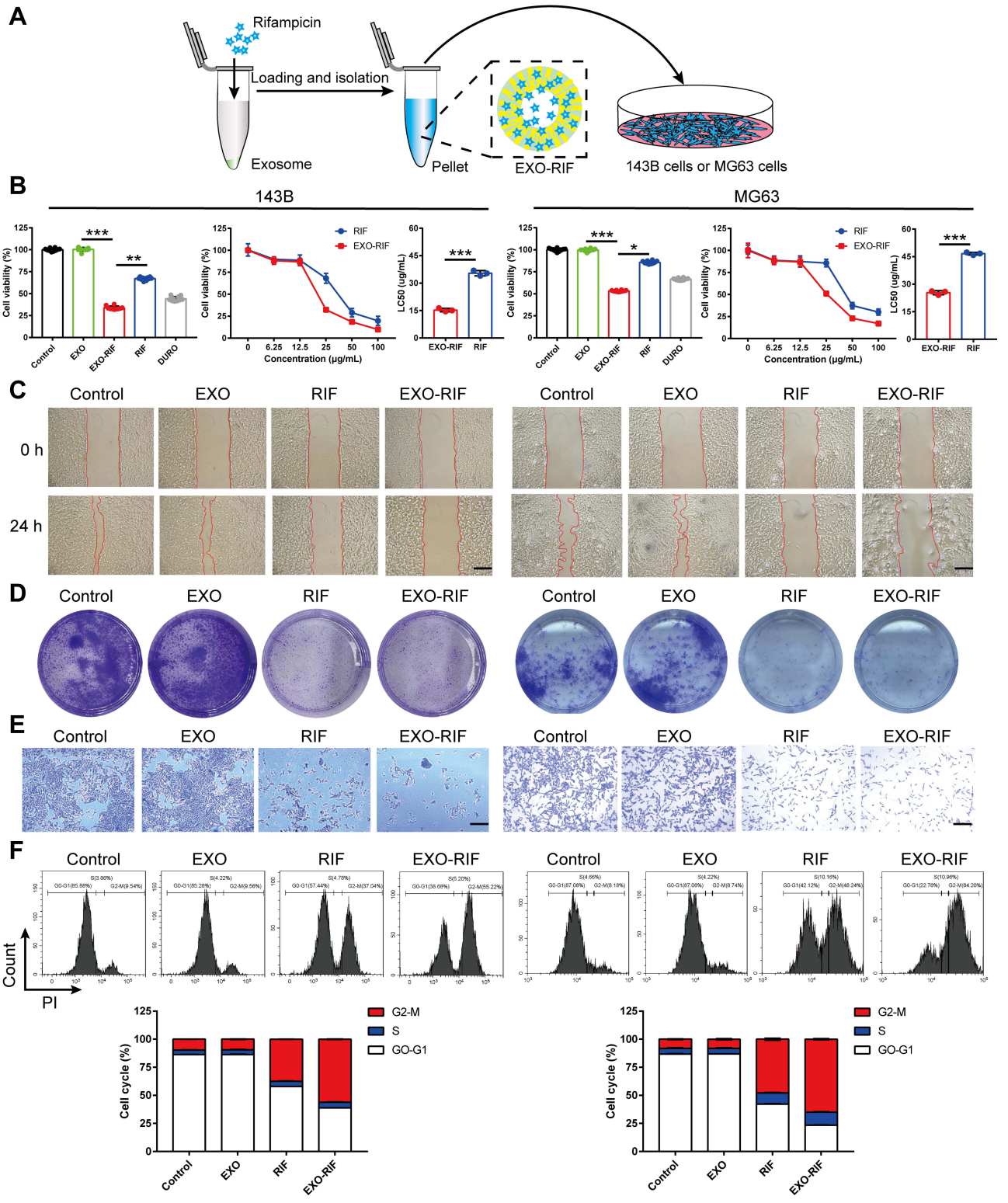

Figure 3 Exosome-Rifampicin induced G2/M phase arrest and cell death in human OS cells. (**A**) Schematic illustration of the experiment. (**B**) Cell viability of OS cells treated with PBS, Exosome, Exosome-Rifampicin, Rifampicin and Doxorubicin. n = 10. (**C**) Representative images of OS cell migration. n = 3. (**D**) Representative images of OS cell Clonogenicity. n = 3. (**E**) Representative Transwell-images of OS cell invasion. n = 3. (**F**) Flow cytometric detection of the cell cycle of osteosarcoma cells. n = 4. *p <0.05, **p <0.01, ***p <0.001.

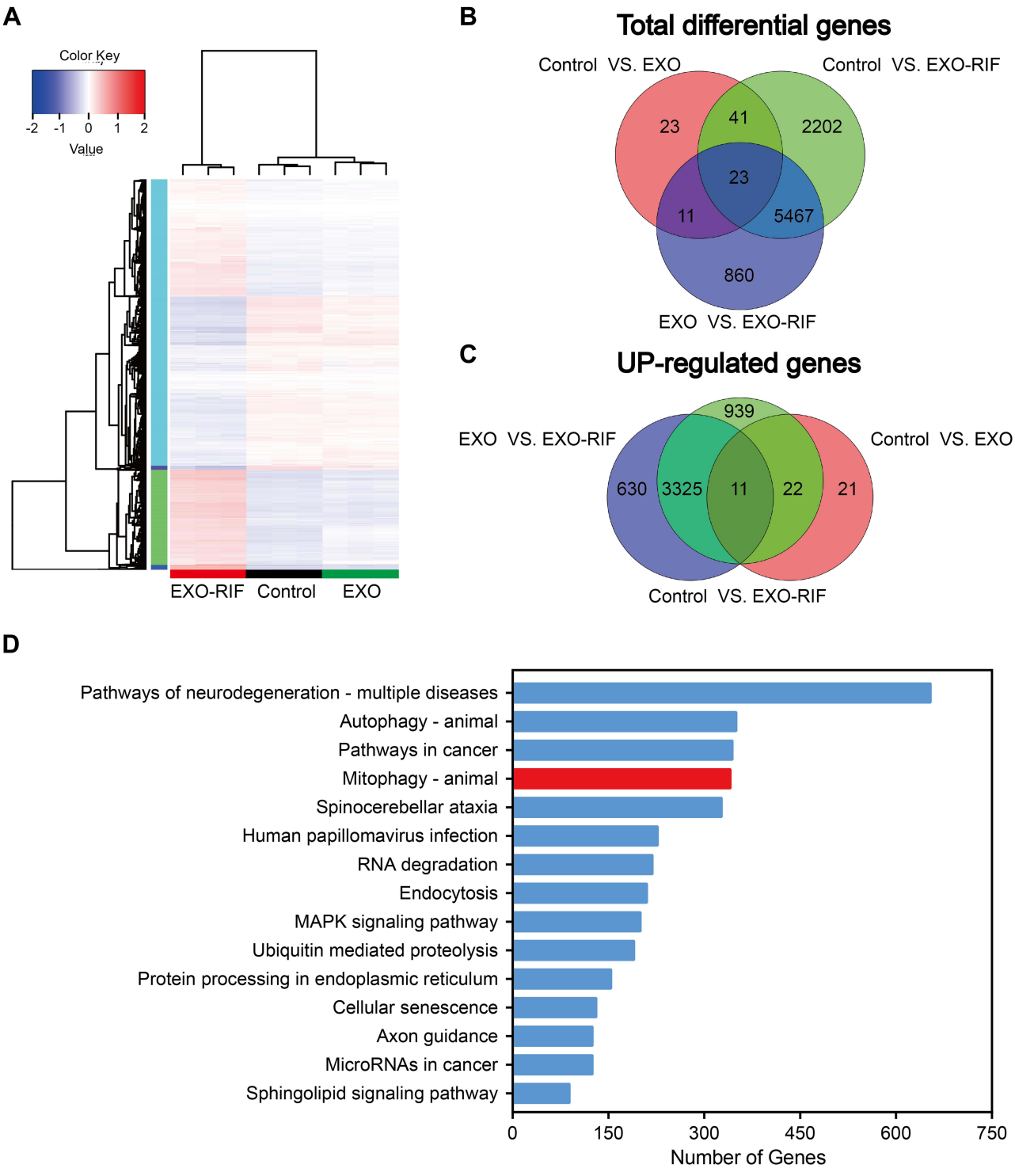

Figure 4 RNA-Seq data with 143B cells treated with PBS, Exosome and Exosome-Rifampicin. (**A**) Heatmap showing the differentially expressed genes in PBS, Exosome and Exosome-Rifampicin treated cells. n = 3. (**B** and **C**) Venn diagram of total differentially expressed and up-regulated genes (DEGs). (**D**) Analysis of altered genes in top categories according to KEGG from Exosome vs Exosome-Rifampicin (fold change ≥ ± 2 and P -value < 0.05).

Exosomes Enhanced RIF Targeting of OS in vivo

EXO-RIF-CY3 was injected intravenously into mice (Figure 7A) and in vivo imaging showed higher drug concentrations for EXO-RIF-CY3 than for RIF-CY3 at the tumor site (Figure 7B) and in the liver, as confirmed by fluorescence imaging of organs (Figure 7C and D).

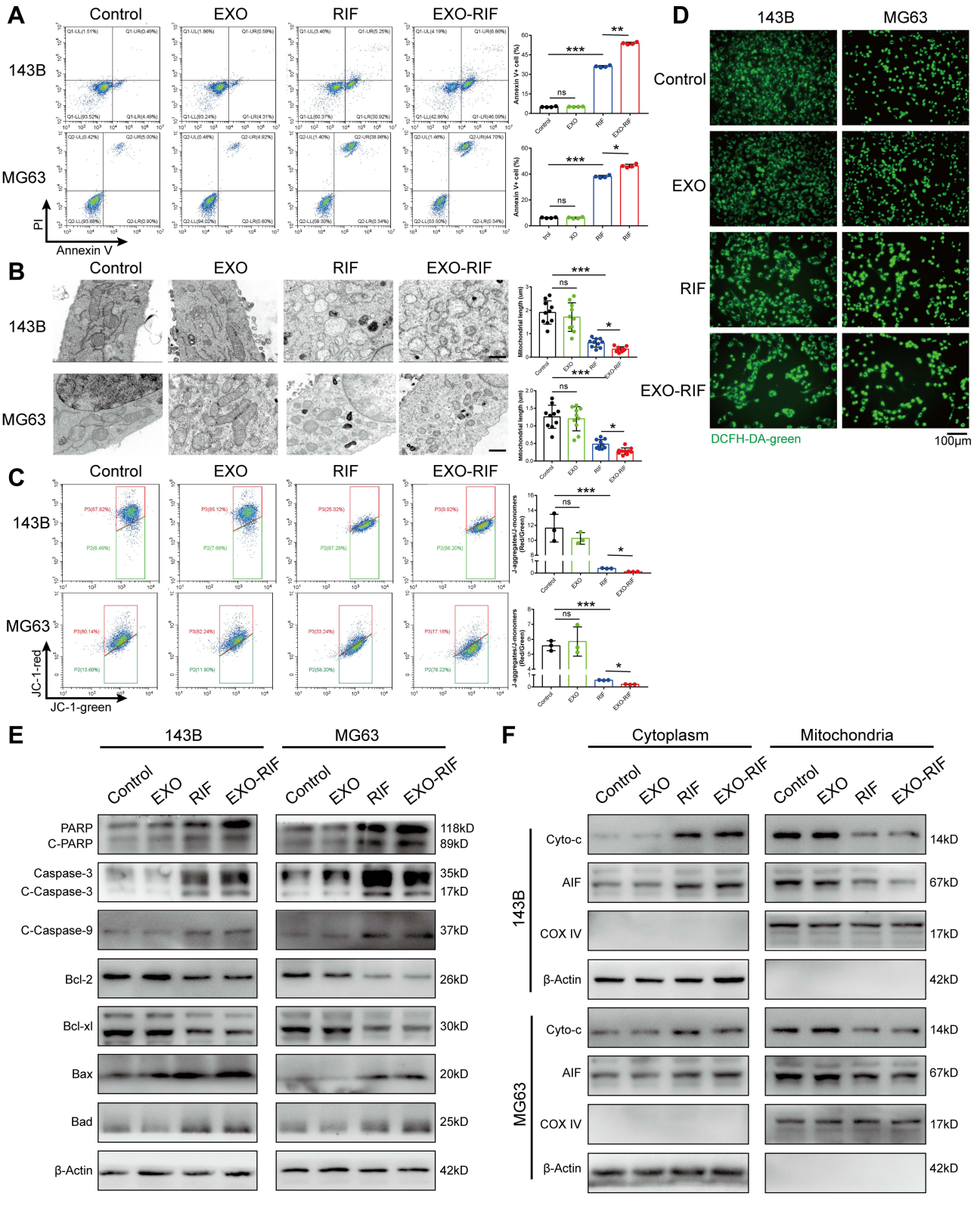

Figure 5 Exosome-Rifampicin induced mitochondrial apoptosis in human OS cells. (**A**) Apoptosis detection by flow cytometry. n = 4. (**B**) Representative picture of mitochondria taken by electron microscope. (**C**) Detection of JC-1 fluorescence in OS cells by flow cytometry. n = 4. (**D**) Fluorescence microscope captures DCFH-DA fluorescence of OS cells. (**E** and **F**) Expression of mitochondrial apoptosis-related proteins was measured by Western blotting. *p <0.05, **p <0.01, ***p <0.001.

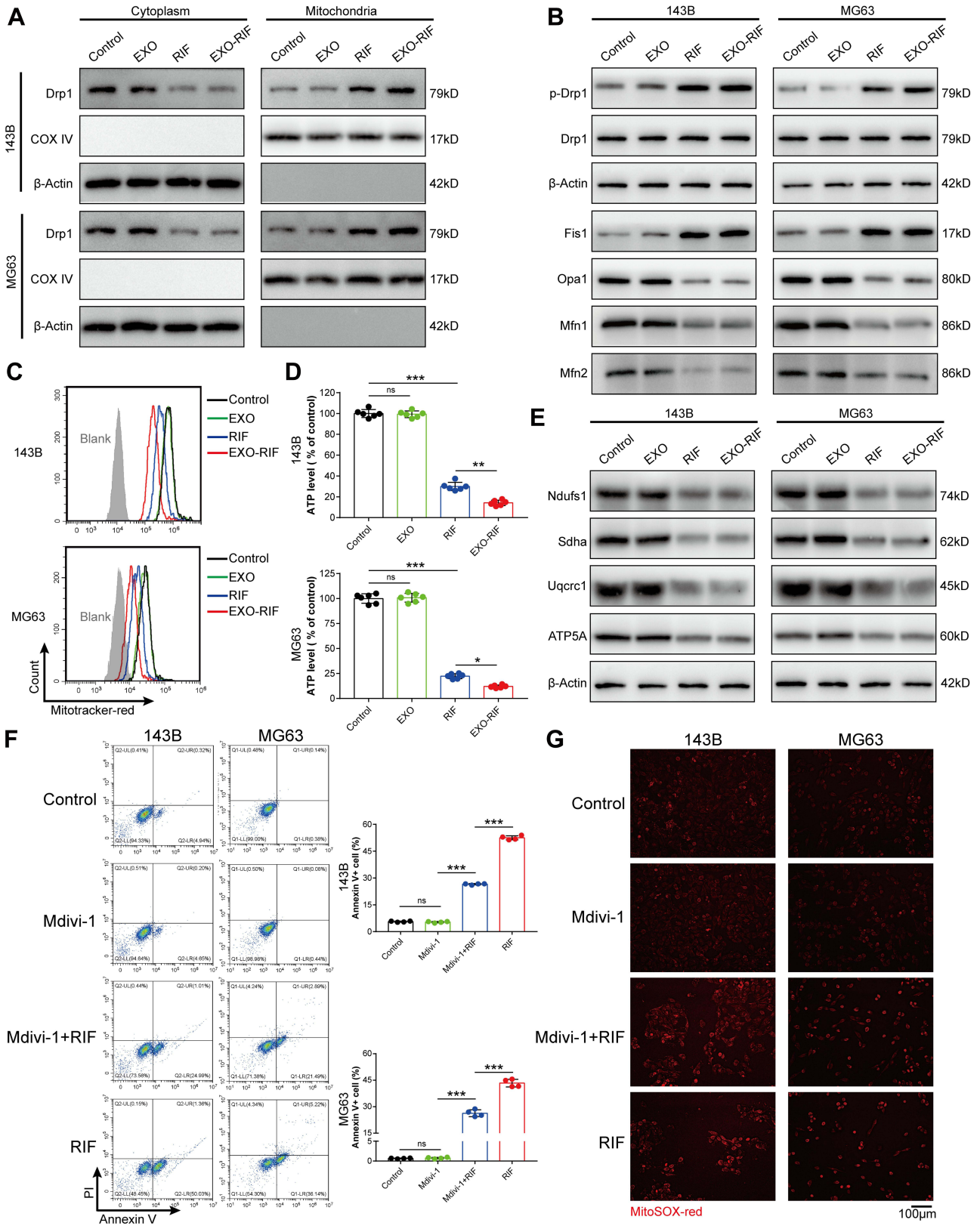

Figure 6 Exosome-Rifampicin activated phosphorylation of Drp1 to induce mitochondrial apoptosis. (**A** and **B**) The effects of Exosome-Rifampicin on mitochondrial fusion/fission protein expression in OS cells. Representative immunoblot of the protein levels of p-Drp1, Drp1, Fis1, Opa1, Mfn1 and Mfn2. n = 3. (**C**) Detection of Mitotracker fluorescence in OS cells by flow cytometry. n = 4. (**D**) ATP levels in OS cells. n = 6. (**E**) Immunoblot analysis of Nudfs1, Sdha, Uqcrc1 and ATP5A. n = 3. (**F**) Apoptosis detection by flow cytometry. n = 4. (**G**) Fluorescence microscopy of MitoSOX fluorescence in OS cells. n = 4. *p <0.05, **p <0.01, ***p <0.001.

https://doi.org/10.2147/IJN.S379917 DovePress

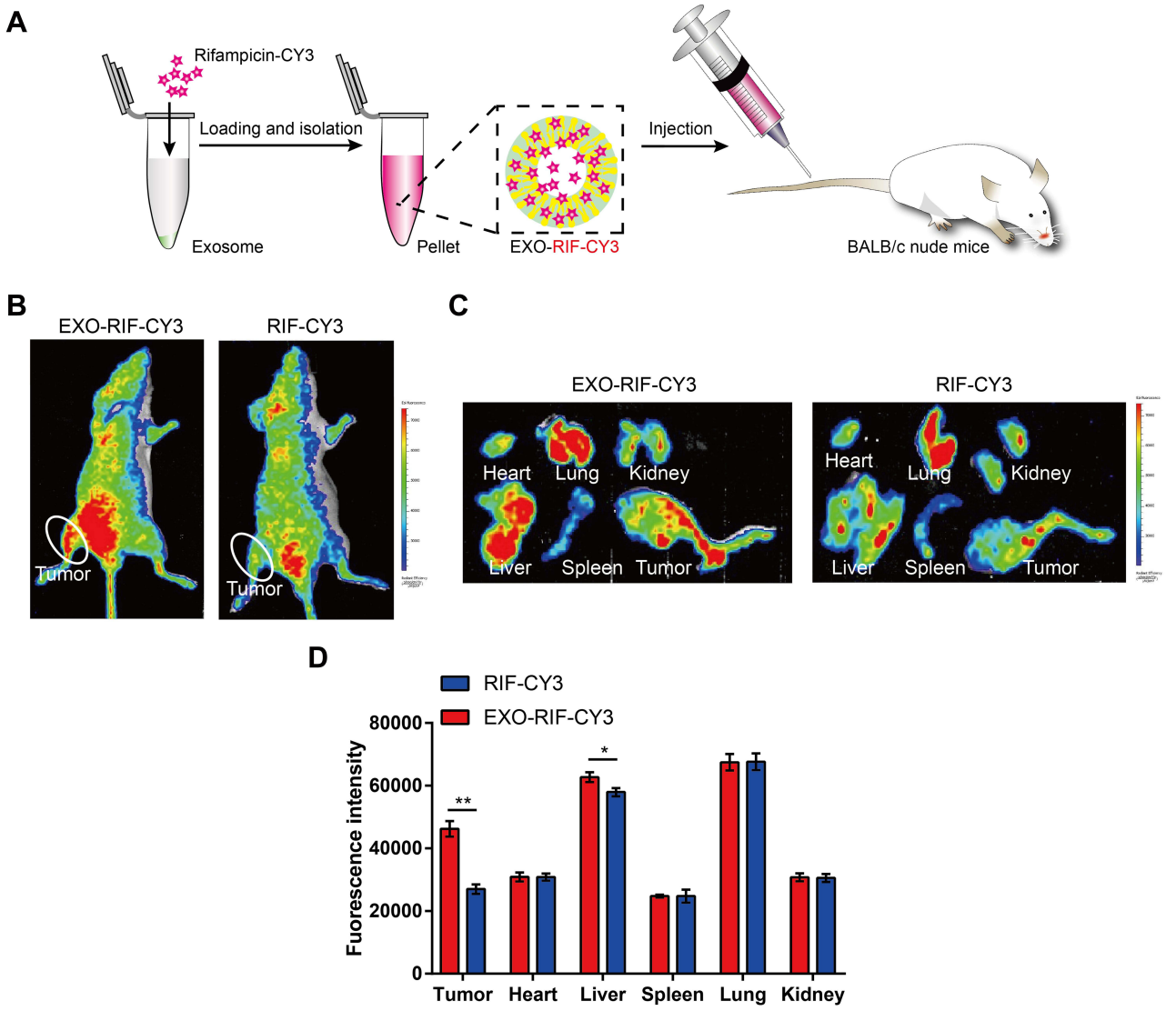

Figure 7 Exosome loading facilitated the targeting of rifampicin to OS cells in vivo. (**A**) Schematic illustration of the experiment. (**B**) In vivo representative fluorescence imaging of tumor-bearing mice with different treatments. (**C** and **D**) Representative fluorescence imaging of mouse organs. n = 3. *p <0.05, **p <0.01.

The Efficacy of EXO-RIF Against OS in vivo

RIF was injected continuously for a period of 21 days, beginning 7 days after 143B tumor cell implantation in 5-week-old nude mice (Figure 8A). EXO-RIF inhibited OS growth with significantly more potency than RIF (Figure 8B–D). Both RIF and EXO-RIF reduced the tumor damage to the bone, as shown by Micro-CT (Figure 8E). RIF and EXO-RIF treated groups showed decreased Ki67 expression, high c-caspase-3 and Bax and low expression of Bcl-2, suggesting inhibition of cell proliferation and promotion of apoptosis (Figure 8F). TUNEL staining indicated that many apoptotic cells were produced in the RIF and EXO-RIF groups (Figure 8G).

RIF and EXO-RIF treated mice lost significantly less weight than controls (Figure 8H) and showed extended survival (mice were sacrificed when tumor volume reached 2000 mm^3). Survival rates were highest in the EXO-RIF group (Figure 8I).

HE staining analysis indicated no significant pathological changes of organ tissues after EXO-RIF treatment and expression of ALT, AST, BUN, Cr, CK and CK-MB were not significantly different from controls (Figure S7). Thus, EXO-RIF had no significant toxicity.

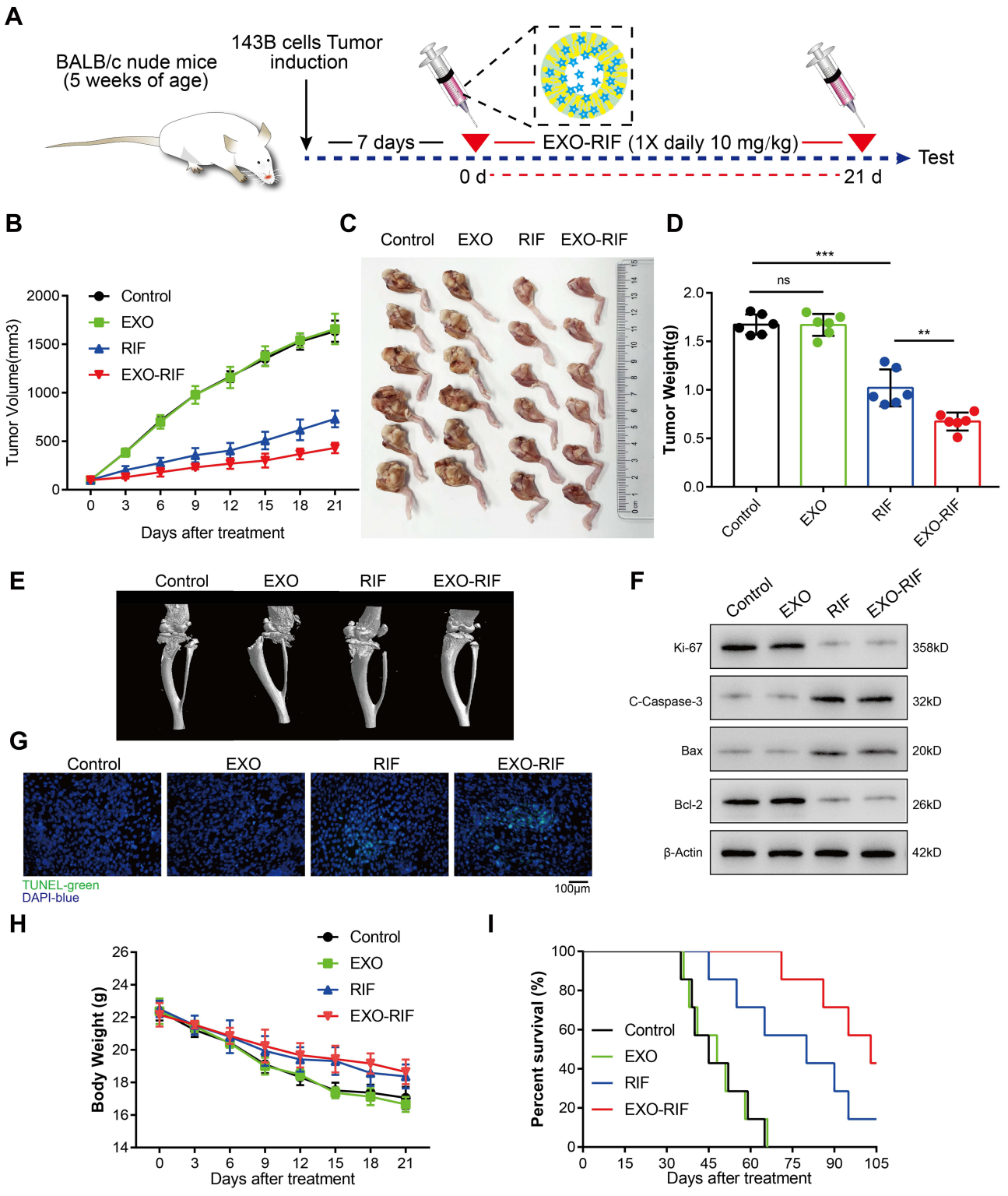

Figure 8 Therapeutic efficacy of Exosome-Rifampicin in vivo. (**A**) Schematic illustration of the experiment. (**B**) Tumor growth curves of tumor volume after different treatments for 21 days. (**C** and **D**) Tumor images and weight of mice with different treatments after 21 days. (**E**) Representative micro-CT imaging of mouse tibia. (**F**) Immunoblot analysis of Ki67, Cleaved-Caspase-3, Bax and Bcl-2. (**G**) Representative TUNEL fluorescence imaging of tumor. (**H** and **I**) Weight changes and survival rates of mice with different treatments. **p <0.01, ***p <0.001.

https://doi.org/10.2147/IJN.S379917 DovePress

Discussion

Long-term survival of OS patients treated with maximal combination therapy is reduced due to early lung metastasis and the development of chemotherapy resistance.[14,23,24] Therefore, the development of targeted therapeutic strategies for systemic tumor control has indisputable clinical significance. Exosomes have the potential to be enriched with therapeutic drugs and delivered to tumor sites for targeted therapy. BMSC-derived exosomes have a high affinity for OS cells.[25,26] Angus J loaded doxorubicin into MSC-EXO using electroporation to reduce metabolic degradation and demonstrated increased accumulation in tumor tissue compared with free doxorubicin.[27] Furthermore, recognition of MSC-EXO membrane receptors by tumor cells may facilitate passive ingestion of cytocidal drugs.[28,29] In addition, tumor targeting may be enhanced by engineering of folate receptors into EXO.[30–32]

We have previously demonstrated that EXO loading increased the rate at which rifampicin entered cells, enhancing the drug's inhibition of OS cell growth and migration. Significant difference in tumor volume was found following EXO-RIF treatment compared with RIF alone and the exosome-loaded drug inhibited the OS-induced destruction of the tibia more effectively. Thus, BMSC-derived EXO may regulate the dynamic balance of osteogenesis and osteoclasts. In addition, the survival rate of mice in the exosome-loading group was higher than that in the free drug group, perhaps because exosome-loading killed tumors that had metastasized to other organs throughout the body. Following this hypothesis, we are currently conducting research on EXO-RIF inhibition of lung metastasis in OS.

Rifampicin is a broad-spectrum antibiotic of the rifamycin family.[33] It binds the β-subunit of DNA-dependent bacterial RNA polymerase, preventing the enzyme from recognizing DNA, thereby blocking transcription and preventing protein synthesis.[34] Maggi et al were the first to synthesize and disclose the drug, rifampicin, in 1966.[10] It has been used to treat tuberculosis during the following 50 years.[35–37] Winters et al reported the in vitro anti-OS effect of rifampicin in

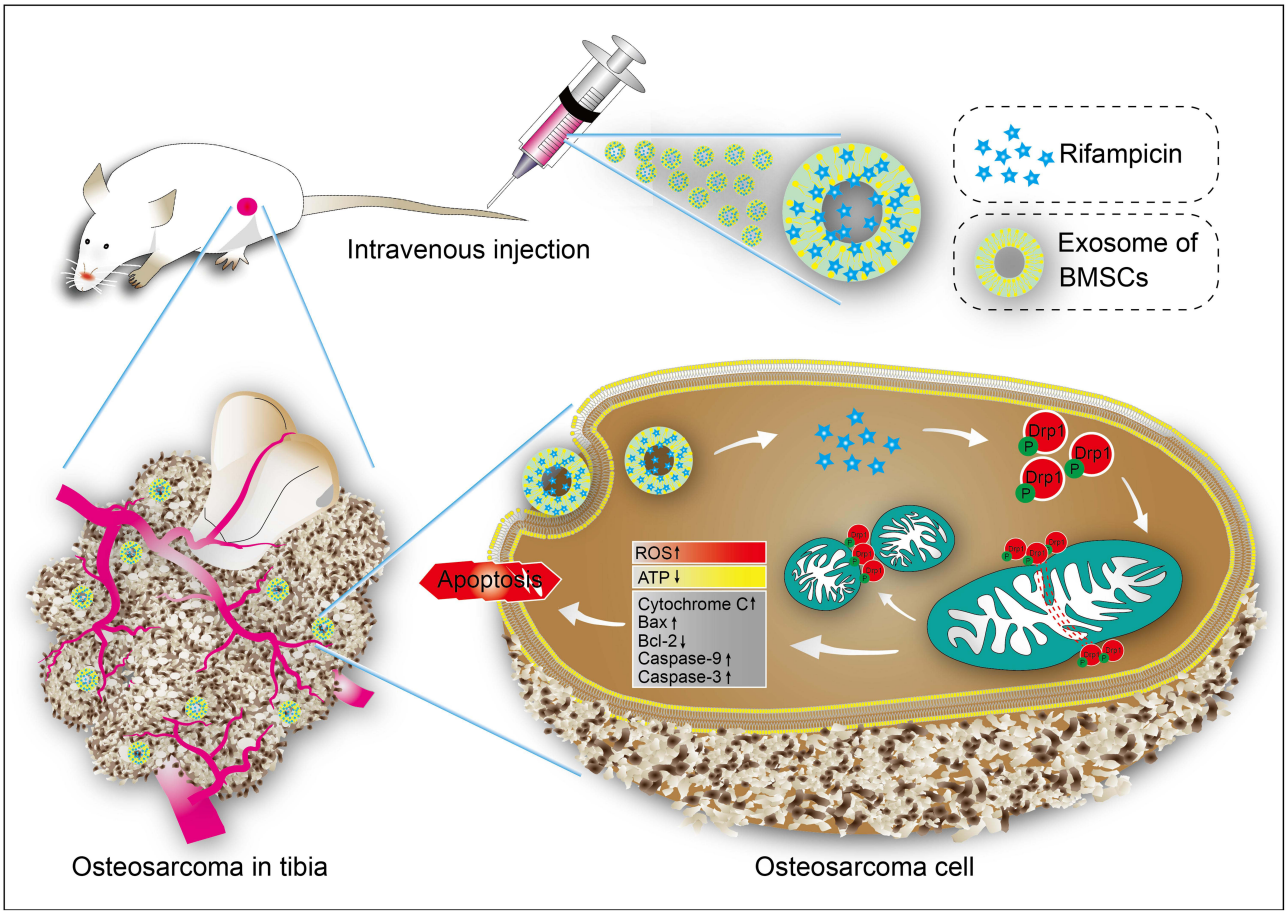

Figure 9 Schematic illustration of Exosome-Rifampicin activated phosphorylation of Drp1 to induce mitochondrial apoptosis in OS cells.

1974 but no mechanistic details were given.[38] To the best of our knowledge, the present study is the first to demonstrate that rifampicin activates Drp1, causing mitochondrial cleavage and triggering mitochondrial apoptosis, and these actions account for its anti-OS effect. Interestingly, RNA-Seq suggested involvement of rifampicin in regulation of autophagy and mitophagy and we are conducting research to follow this up.

A significant therapeutic effect on OS both in vitro and in vivo has been demonstrated but further experimental studies are needed. For example, the specific target of rifampicin's anti-OS effect needs to be identified, an attractive future research project. Whether exosome drug delivery affects drug metabolism in vivo also requires elucidation.

Conclusion

In conclusion, rifampicin was a highly potent Drp1 agonist that caused mitochondrial cleavage and triggered apoptosis, accounting for its anti-OS effect. Engineered exosome-rifampicin displayed potent antitumor therapeutic effects with remarkably low toxicity (Figure 9). Exosome-rifampicin nanoparticles appear to offer a promising strategy for the treatment of malignant tumors.

Acknowledgments

We sincerely appreciate the contributions of all laboratory members. This work was supported by the Program of the National Natural Science Foundation of China (No. 82074233 and 81771323) and Scientific Research Foundation for Advanced Talents, Xiang'an hospital of Xiamen university (No. PM201809170009). This work was also supported by Guangdong Basic and Applied Basic Research Foundation (No. 2021A1515010722), Science and Technology Planning Project of Shenzhen Municipality (No. JCYJ20190813112401660) and the Natural Science Foundation of Fujian Province of China (No. 2022J01018).

Disclosure

The authors report no conflicts of interest in this work.

References

1. Meltzer PS, Helman LJ, Longo DL. New horizons in the treatment of osteosarcoma. *N Engl J Med*. 2021;385(22):2066–2076. doi:10.1056/NEJMra2103423
2. Gill J, Gorlick R. Advancing therapy for osteosarcoma. *Nat Rev Clin Oncol*. 2021;18(10):609–624. doi:10.1038/s41571-021-00519-8
3. Brookes MJ, Chan CD, Baljer B, et al. Surgical advances in osteosarcoma. *Cancers*. 2021;13(3):388. doi:10.3390/cancers13030388
4. Marchandet L, Lallier M, Charrier C, Baud'huin M, Ory B, Lamoureux F. Mechanisms of resistance to conventional therapies for osteosarcoma. *Cancers*. 2021;13(4):683. doi:10.3390/cancers13040683
5. Smrke A, Anderson PM, Gulia A, Gennatas S, Huang PH, Jones RL. Future directions in the treatment of osteosarcoma. *Cells*. 2021;10(1):172. doi:10.3390/cells10010172
6. Chen C, Xie L, Ren T, Huang Y, Xu J, Guo W. Immunotherapy for osteosarcoma: fundamental mechanism, rationale, and recent breakthroughs. *Cancer Lett*. 2021;500:1–10. doi:10.1016/j.canlet.2020.12.024
7. Yang C, Tian Y, Zhao F, et al. Bone microenvironment and osteosarcoma metastasis. *Int J Mol Sci*. 2020;21(19). doi:10.3390/ijms21196985
8. Richardus JH, Tiwari A, Barth-Jaeggi T, et al. Leprosy post-exposure prophylaxis with single-dose rifampicin (LPEP): an international feasibility programme. *Lancet Glob Health*. 2021;9(1):e81–e90. doi:10.1016/S2214-109X(20)30396-X
9. Mieras L, Anthony R, van Brakel W, et al. Negligible risk of inducing resistance in Mycobacterium tuberculosis with single-dose rifampicin as post-exposure prophylaxis for leprosy. *Infect Dis Poverty*. 2016;5(1):46. doi:10.1186/s40249-016-0140-y
10. Maggi N, Pasqualucci CR, Ballotta R, Sensi P. Rifampicin: a new orally active rifamycin. *Chemotherapy*. 1966;11(5):285–292. doi:10.1159/000220462
11. Rezabakhsh A, Sokullu E, Rahbarghazi R. Applications, challenges and prospects of mesenchymal stem cell exosomes in regenerative medicine. *Stem Cell Res Ther*. 2021;12(1):521. doi:10.1186/s13287-021-02596-z
12. Choi H, Choi K, Kim DH, et al. Strategies for targeted delivery of exosomes to the brain: advantages and challenges. *Pharmaceutics*. 2022;14(3):672. doi:10.3390/pharmaceutics14030672
13. Zhou B, Xu K, Zheng X, et al. Application of exosomes as liquid biopsy in clinical diagnosis. *Signal Transduct Target Ther*. 2020;5(1):144. doi:10.1038/s41392-020-00258-9
14. Kamerkar S, LeBleu VS, Sugimoto H, et al. Exosomes facilitate therapeutic targeting of oncogenic KRAS in pancreatic cancer. *Nature*. 2017;546(7659):498–503. doi:10.1038/nature22341
15. Kalluri R, LeBleu VS. The biology, function, and biomedical applications of exosomes. *Science*. 2020;367(6478). doi:10.1126/science.aau6977
16. Wang S, Li F, Ye T, et al. Macrophage-tumor chimeric exosomes accumulate in lymph node and tumor to activate the immune response and the tumor microenvironment. *Sci Transl Med*. 2021;13(615):eabb6981. doi:10.1126/scitranslmed.abb6981
17. Semcheddine F, El Islem Guissi N, Liu W, et al. Rapid and label-free cancer theranostics via in situ bio-self-assembled DNA-gold nanostructures loaded exosomes. *Mater Horiz*. 2021;8(10):2771–2784. doi:10.1039/d1mh00880c

18. Chen J, Song Y, Miao F, et al. PDL1-positive exosomes suppress antitumor immunity by inducing tumor-specific CD8(+) T cell exhaustion during metastasis. *Cancer Sci*. 2021;112(9):3437–3454. doi:10.1111/cas.15033
19. Kim MS, Haney MJ, Zhao Y, et al. Development of exosome-encapsulated paclitaxel to overcome MDR in cancer cells. *Nanomedicine*. 2016;12 (3):655–664. doi:10.1016/j.nano.2015.10.012
20. Yuan X, Amarnath Praphakar R, Munusamy MA, Alarfaj AA, Suresh Kumar S, Rajan M. Mucoadhesive guargum hydrogel inter-connected chitosan-g-polycaprolactone micelles for rifampicin delivery. *Carbohydr Polym*. 2019;206:1–10. doi:10.1016/j.carbpol.2018.10.098
21. Huang Z, Chen H, Wang S, et al. NLRP3 overexpression associated with poor prognosis and presented as an effective therapeutic target in osteosarcoma. *Front Pharmacol*. 2021;12:724923. doi:10.3389/fphar.2021.724923
22. Senerchia AA, Macedo CR, Ferman S, et al. Results of a randomized, prospective clinical trial evaluating metronomic chemotherapy in nonmetastatic patients with high-grade, operable osteosarcomas of the extremities: a report from the Latin American group of osteosarcoma treatment. *Cancer*. 2017;123(6):1003–1010. doi:10.1002/cncr.30411
23. Gonzalez-Fernandez Y, Imbuluzqueta E, Zalacain M, Mollinedo F, Patino-Garcia A, Blanco-Prieto MJ. Doxorubicin and edelfosine lipid nanoparticles are effective acting synergistically against drug-resistant osteosarcoma cancer cells. *Cancer Lett*. 2017;388:262–268. doi:10.1016/j.canlet.2016.12.012
24. Zhang H, Wang J, Ren T, et al. Bone marrow mesenchymal stem cell-derived exosomal miR-206 inhibits osteosarcoma progression by targeting TRA2B. *Cancer Lett*. 2020;490:54–65. doi:10.1016/j.canlet.2020.07.008
25. Zhao W, Qin P, Zhang D, et al. Long non-coding RNA PVT1 encapsulated in bone marrow mesenchymal stem cell-derived exosomes promotes osteosarcoma growth and metastasis by stabilizing ERG and sponging miR-183-5p. *Aging*. 2019;11(21):9581–9596. doi:10.18632/aging.102406
26. Lennaard AJ, Mamand DR, Wiklander RJ, El Andaloussi S, Wiklander OPB. Optimised electroporation for loading of extracellular vesicles with doxorubicin. *Pharmaceutics*. 2021;14(1):38. doi:10.3390/pharmaceutics14010038
27. Garnier D, Ratcliffe E, Briand J, Cartron PF, Oliver L, Vallette FM. The activation of mesenchymal stem cells by glioblastoma microvesicles alters their exosomal secretion of miR-100-5p, miR-9-5p and let-7d-5p. *Biomedicines*. 2022;10(1):112. doi:10.3390/biomedicines10010112
28. Zhou W, Zhou Y, Chen X, et al. Pancreatic cancer-targeting exosomes for enhancing immunotherapy and reprogramming tumor microenvironment. *Biomaterials*. 2021;268:120546. doi:10.1016/j.biomaterials.2020.120546
29. Rao D, Huang D, Sang C, Zhong T, Zhang Z, Tang Z. Advances in mesenchymal stem cell-derived exosomes as drug delivery vehicles. *Front Bioeng Biotechnol*. 2022;9:797359. doi:10.3389/fbioe.2021.797359
30. Luo T, von der Ohe J, Hass R. MSC-derived extracellular vesicles in tumors and therapy. *Cancers*. 2021;13(20):5212. doi:10.3390/cancers13205212
31. Du J, Wan Z, Wang C, et al. Designer exosomes for targeted and efficient ferroptosis induction in cancer via chemo-photodynamic therapy. *Theranostics*. 2021;11(17):8185–8196. doi:10.7150/thno.59121
32. Thwaites GE, Scarborough M, Szubert A, et al. Adjunctive rifampicin for Staphylococcus aureus bacteraemia (ARREST): a multicentre, randomised, double-blind, placebo-controlled trial. *Lancet*. 2018;391(10121):668–678. doi:10.1016/S0140-6736(17)32456-X
33. Verma R, Gurumurthy M, Yeo BCM, Lu Q, Naftalin CM, Paton NI. Effects of increasing concentrations of rifampicin on different mycobacterium tuberculosis lineages in a whole-blood bactericidal activity assay. *Antimicrob Agents Chemother*. 2022;66(2):e0169921. doi:10.1128/AAC.01699-21
34. Garcia-Prats AJ, Svensson EM, Winckler J, et al. Pharmacokinetics and safety of high-dose rifampicin in children with TB: the Opti-Rif trial. *J Antimicrob Chemother*. 2021;76(12):3237–3246. doi:10.1093/jac/dkab336
35. Dooley KE, Rosenkranz SL, Conradie F, et al. QT effects of bedaquiline, delamanid, or both in patients with rifampicin-resistant tuberculosis: a Phase 2, open-label, randomised, controlled trial. *Lancet Infect Dis*. 2021;21(7):975–983. doi:10.1016/S1473-3099(20)30770-2
36. Lilic M, Chen J, Boyaci H, et al. The antibiotic sorangicin A inhibits promoter DNA unwinding in a Mycobacterium tuberculosis rifampicin-resistant RNA polymerase. *Proc Natl Acad Sci U S A*. 2020;117(48):30423–30432. doi:10.1073/pnas.2013706117
37. Winters, WD, Tuan, AL, Morton, DL Differential effects of rifampicin on cultured human tumor cells *Cancer Res* 1974; 34 (12): 3173–3179. doi:10.1016/0065-2571(75)90011-4
38. Shichiri M, Fukai N, Kono Y, Tanaka Y. Rifampicin as an oral angiogenesis inhibitor targeting hepatic cancers. *Cancer Res*. 2009;69 (11):4760–4768. doi:10.1158/0008-5472.Can-08-3417